First-principles calculation of the lattice thermal conductivities of α-, β-, and γ-$\mathrm{Si_3N_4}$

Kazuyoshi Tatsumi,[1, 2, ∗] Atsushi Togo,[2] and Isao Tanaka[2, 3, 4]

[1] aAdvanced Measurement Technology Center, Institute of Materials and Systems for Sustainability,
Nagoya University, Chikusa, Nagoya 464-8603, Japan
[2] Center for Elements Strategy Initiative for Structural Materials,
Kyoto University, Sakyo, Kyoto 606-8501, Japan
[3] Department of Materials Science and Engineering,
Kyoto University, Sakyo, Kyoto 606-8501, Japan
[4] Nanostructures Research Laboratory, Japan Fine Ceramics Center, Atsuta, Nagoya 456-8587, Japan

Lattice thermal conductivities of α-, β- and γ-$\mathrm{Si_3N_4}$ single crystals are investigated from *ab-initio* anharmonic lattice dynamics, within the single-mode relaxation-time approximation of the linearized phonon Boltzmann transport equation. At 300 K, the lattice thermal conductivity of α-$\mathrm{Si_3N_4}$ is calculated as $\kappa_{xx} = 69$ and $\kappa_{zz} = 99$ (in units of $\mathrm{Wm^{-1}K^{-1}}$). For β-$\mathrm{Si_3N_4}$, $\kappa_{xx} = 73$ and $\kappa_{zz} = 198$ are obtained, that is consistent with the reported experimental values of 69 and 180, respectively. The difference of anisotropy between α-$\mathrm{Si_3N_4}$ and β-$\mathrm{Si_3N_4}$ is originated from their characteristic difference in the phonon band structures, although their crystal structures are similar in their local atomic coordinates. In α-$\mathrm{Si_3N_4}$, acoustic-mode phonons below 6 THz are the main heat carriers. In β-$\mathrm{Si_3N_4}$, the phonon modes up to 12 THz contribute to the lattice thermal conductivity. In γ-$\mathrm{Si_3N_4}$, $\kappa = 81$ is obtained. The distribution of phonon mode contributions to lattice thermal conductivity along phonon frequency is found to closely resemble κ_{xx} of β-$\mathrm{Si_3N_4}$ although the phonon lifetimes of γ-$\mathrm{Si_3N_4}$ are twice shorter than those of β-$\mathrm{Si_3N_4}$.

I. INTRODUCTION

Several nitride insulators showing good thermal conductivities are important for heat sink materials used at elevated temperatures. Wurtzite-type w-AlN, which has an Adamantine (diamond-like) crystal structure, was noted by Slack et al.[1] as exhibiting a large thermal conductivity of over 100 $\mathrm{WK^{-1}m^{-1}}$. $\mathrm{Si_3N_4}$ has been more recently recognized as one of the good thermally conductive insulators. Remarkable advances in technologies related to the densification of the ceramic body and microstructural control have pushed the thermal conductivities of $\mathrm{Si_3N_4}$ ceramics up to 177 $\mathrm{WK^{-1}m^{-1}}$.[2–5] Since $\mathrm{Si_3N_4}$ ceramics also exhibit high mechanical strength at elevated temperatures, they are regarded as ideal for use in various applications, such as engine components, gas turbines, and heat sink substrates of power semiconductor devices.

At atmospheric pressure, $\mathrm{Si_3N_4}$ exists in one of two phases, α and β, both in the hexagonal lattice system, which are generally considered to be low- and high-temperature phases, respectively.[2,5,6] Their crystal structures are commonly formed by stacking of basal layers of $\mathrm{SiN^4}$ tetrahedra. The stacking manners in α and β-$\mathrm{Si_3N_4}$ are as ABAB.. and ABCDABCD.., respectively, where the CD layers are mirror images of AB with respect to the plane.[7] The unit cell periodicity of the α phase is approximately two times longer than that of the β phase, with lattice constants of c = 5.62^8 and 2.91^9 Å, respectively. In addition to the α and β phases, the cubic spinel γ-$\mathrm{Si_3N_4}$ can be obtained upon compression and simultaneous-in-situ heating.[10,11] The reported transition pressures were scattered from 10 to 36 GPa depending on the experimental conditions. The produced γ phase can be experimentally quenched to atmospheric pressure and room temperature.

By using high-resolution thermoreflectance microscopy, Li *et al.*[12] reported the thermal conductivities of individual rod-shaped β-$\mathrm{Si_3N_4}$ grains in a ceramic to be 69 and 180 $\mathrm{Wm^{-1}K^{-1}}$ along the *a* and *c* axes, respectively, and thus revealed the large anisotropy in thermal conductivity. Takahashi *et al.*[13] recently developed a technique whereby β-$\mathrm{Si_3N_4}$ grains are coated with graphene of relatively high magnetic susceptibility, enabling them to align their c axes along the external magnetic field. Based on this large anisotropy in thermal conductivity, it was proposed that the textural structure of rod-shaped β-$\mathrm{Si_3N_4}$ grains would increase their thermal conductivity to a level matching or exceeding that of w-AlN.

Although the fabrication of millimeter-sized β-$\mathrm{Si_3N_4}$ single crystals has been reported[14], the thermal conductivity of no isolated single crystal of any $\mathrm{Si_3N_4}$ phase has yet been experimentally determined. It was proposed[15] that the anisotropy in the thermal conductivity of β-$\mathrm{Si_3N_4}$ phase grains may not stem from the intrinsic crystal properties, but rather, from the selective removal of crystal defects along the c axis of the grains. Theoretically, Hirosaki *et al.*[16] estimated the room-temperature lattice thermal conductivities (LTCs) κ_{xx} and κ_{zz} of α-$\mathrm{Si_3N_4}$ to be 105 and 225, and κ_{xx} and κ_{zz} of β-$\mathrm{Si_3N_4}$ to be 170 and 450, respectively, by applying the Green-Kubo formulation to the molecular dynamics method with the interatomic potentials proposed by Vashishta *et al.* The ratio of the LTCs along the a and c axes agreed well with the experimental results obtained by Li *et al.*; however, the absolute values were more than two times larger than the experimental results. The LTC of the γ phase was estimated only by the Slack model.[17] While the thermal conductivity of polycrystalline β-$\mathrm{Si_3N_4}$ has been signifi-

cantly improved[2–5], our basic knowledge of, for example, the thermal conductivity tensors of the different crystal phases remains insufficient.

A decade ago, *ab-initio* calculations based on Boltzmann transport theory combined with the harmonic and anharmonic interatomic force constants by density functional theory were presented by Broido *et al.*.[18] Because of the computational costs, the calculated materials were limited for several crystals having a few atoms in the unit-cell. Semi-empirical approaches with *ab-initio* harmonic phonon states were adopted to understand underlying mechanisms of phonon transport of relatively large systems, whose thermal conductivity was supposed to be experimentally clarified.[19] Thanks to the increasing computational power, the larger systems containing more than 20 atoms per unit-cell have been investigated[?] by the full *ab-initio* calculations within the single-mode relaxation time approximation (RTA).[20,21] This approach gives systematic estimations for LTCs of the large systems whose intrinsic LTCs are not experimentally established and the full solution of Boltzmann transport equation is still difficult to be calculated due to the computational cost. The Si_3N_4 polymorphs, which contain 14 or 28 atoms per primitive cell, are the case.

The *ab-initio* LTC approach has many crystalline systems whose underlying mechanisms of the phonon thermal transport are still not clarified. The *ab-initio* LTC calculation can now be applied to the other larger systems. The previous study of the LTC in many polymorphs of the zincblende and wurtzite structures showed that the difference in the stacking orders of the atom planes between these structures affects little their LTC values.[22] On the other hand, the previous experimental[5,23] and theoretical[16,17] studies of thermal conductivities of α- and β-Si_3N_4 suggest that this is not true for α- and β-Si_3N_4. While the point group symmetry determines the anisotropy of LTC tensors, the degree of the anisotropy depends on the material, which can be examined by the first principles LTC calculation as the case of $Ge_2Sb_2Te_5$ in ref. 24. γ-Si_3N_4 can be regarded as an ideally simple representative of the spinel-type structure, because it has a single non-transition metal element for cations. By comparing the γ phase with the α/β phases, we can shed light on the underling mechanisms of the LTC of the spinel-type structure.

The present study aims to qualitatively understand the LTC tensors among the three Si_3N_4 phases by means of the *ab-initio* approach. After the methodology section, we examine the validity of the present LTC results first. Then the harmonic phonon states and phonon lifetimes are examined to find what microscopic property determines the characteristics in the LTC.

II. COMPUTATIONAL PROCEDURES

A. Lattice thermal conductivity calculation

The LTCs were calculated by solving the linearized Boltzmann transport equation (LBTE) within the single-mode RTA. We also tried the direct-solution of LBTE35 and shortly leave its calculated LTC values in the following section. However the difference of LTCs between by the single-mode RTA and by the direct solution was found minor for our discussion. Therefore we limited our research based on the single-mode RTA to take advantage of the intuitive closed form of LTCs with the single-mode RTA.

In the following sections, we denote a phonon mode by $\lambda = (\mathbf{q}, p)$ by the set of the phonon wave vector $\mathbf{q}$ and band index p. the relaxation time due to phonon-phonon scattering was obtained as reciprocal of linewidth, $\tau_{\lambda,\text{ph-ph}} = (2\Gamma_\lambda)^{-1}$, where the linewidth that we employed in this study is as follows:

$$\Gamma_\lambda = \frac{18\pi}{\hbar^2} \sum_{\lambda'\lambda''} \left|\Phi_{-\lambda\lambda'\lambda''}\right|^2 \times$$

$$\{(n_{\lambda'} + n_{\lambda''} + 1)\delta(\omega_\lambda - \omega_{\lambda'} - \omega_{\lambda''}) +$$
$$(n_{\lambda'} - n_{\lambda''})\left[\delta(\omega_\lambda + \omega_{\lambda'} - \omega_{\lambda''}) - \delta(\omega_\lambda - \omega_{\lambda'} + \omega_{\lambda''})\right]\}. \tag{1}$$

Here ω_λ is the harmonic phonon frequency of the phonon mode λ, $n_\lambda = [\exp(\hbar\omega_\lambda/k_B T) - 1]^{-1}$ shows the Bose-Einstein distribution, and $\Phi_{\lambda\lambda'\lambda''}$ denotes the three-phonon-scattering strength. $\Phi_{\lambda\lambda'\lambda''}$ was obtained by usual coordinate transformation of third-order force constants from direct space to phonon space.[22] The second- and third-order real-space force constants were obtained from the *ab-initio* calculation, whose details are written in the next section.

In order to compare the more realistic results of the calculated LTC with the experimental data, the isotopic scattering effect due to the natural isotope distribution was taken into account according to the second-order perturbation theory.[25] With the relaxation times of the phonon-phonon scattering and isotropic scattering, $\tau_{\lambda,\text{ph-ph}}$ and $\tau_{\lambda,\text{iso}}$, the total relaxation time for a phonon mode was assumed to be $1/\tau_\lambda = 1/\tau_{\lambda,\text{ph-ph}} + 1/\tau_{\lambda,\text{iso}}$, according to Matthiessen's rule.

These LTCs were calculated with the phonon-phonon interaction calculation code PHONO3PY[22], while the harmonic phonon states were analyzed with the phonon calculation code PHONOPY[26]. These codes have been developed and maintained by the authors in this study.

The available experimental thermal conductivity data of the Si_3N_3 system have been measured on the polycrystalline samples and not measured from any single crystals. In order to consider the effect of various lattice defects in the polycrystalline samples, such as grain boundaries, impurities, and vacancies, we crudely took them into account by a relaxation time $\tau_{\lambda,\text{bs}} = L/|\mathbf{v}_\lambda|$ of a phonon boundary scattering model, where $\mathbf{v}_\lambda = \nabla_\mathbf{q}\omega_\lambda$

is the group velocity and L a parameter regarding to the boundary mean free path. We consider $\tau_{\lambda,\mathrm{bs}}$ as a variable parameter and included it to LTCs according to Matthiessen's rule.

The closed form of the LTC tensors within RTA were obtained via

$$\boldsymbol{\kappa}(T) = \frac{1}{N_\mathbf{q}\Omega} \sum_\lambda \tau_\lambda(T)\mathbf{v}_\lambda \otimes \mathbf{v}_\lambda c_\lambda(T), \qquad (2)$$

where T is the temperature, $N_\mathbf{q}$ is the number of $\mathbf{q}$-points, Ω is the unit cell volume, and c_λ is the mode heat capacity. To analyze the LTC in detail, we calculate the cumulative thermal conductivity:

$$\boldsymbol{\kappa}^\mathrm{c}(\omega) = \frac{1}{N_\mathbf{q}\Omega} \int_0^\omega \sum_\lambda \tau_\lambda(T)\mathbf{v}_\lambda \otimes \mathbf{v}_\lambda c_\lambda(T)\delta(\omega' - \omega)d\omega'. \tag{3}$$

B. Computational details

The IFCs were calculated using the first-principles projector augmented wave method[27] (VASP code[28–30]). The generalized gradient approximation (GGA) parameterized by Perdew, Burke, and Ernzerhof[31] was used for the exchange correlation potential. A plane wave energy cutoff of 500 eV was employed. The crystal structures were optimized until the convergence in the residual forces acting on the constituent atoms was less than 10^{-6} eV/Å. The structural optimization was firstly performed for a temperature of 0 K and 0 GPa. Here the temperature and pressure were considered only for the electronic system and the zero point lattice vibration was not taken into account. The calculated lattice parameters were $a = 7.808$ Å and $c = 5.659$ Å for the α phase, $a = 7.660$ Å and $c = 2.925$ Å for the β phase, and $a = 7.787$ Å for the γ phase, which agree with the experimental data[8;9;32] within +0.7 % errors. The lattice volume optimized at 0 K and 0 GPa within the local density approximation (LDA)[33] for the exchange correlation potential was 143.8 Å^3 for β-Si$_3$N$_4$, being 3 % smaller than the volume with GGA, which is a typical volume contraction of LDA. In our test using β-Si$_3$N$_4$ at 0 K and 0 GPa showed that the LTC calculated with LDA was larger by 2.6 % than that with GGA. For our discussion, these difference is enough small, therefore the impact of choice of exchange correlation potential is considered to be minor in our study.

Supercell and finite difference approaches were used to calculate the IFCs.[34] The $1\times1\times2$, $1\times1\times3$, and $1\times1\times1$ supercells of the conventional unit cells were adopted for the third-order IFCs of the α, β, and γ phases, respectively, while the larger supercells $3\times3\times4$, $3\times3\times8$ and $2\times2\times2$ were adopted for the respective second-order IFCs. The constant atomic displacement distance was set to 0.03 Å. Table I shows the calculated LTC values for several different choices of supercell sizes, indicating that our calculated LTCs are reasonably converging with respect to the supercell sizes.

TABLE I. Calculated lattice thermal conductivities (LTC) of α-, β-, and γ-Si$_3$N$_4$ (WK^{-1}m^{-1}) at 300 K with respect to several combinations of supercell sizes.

Phase	Supercell (# of atoms)		LTC	
	3$^\mathrm{rd}$ FC	2$^\mathrm{nd}$ FC	xx	zz
α	$1\times1\times1$ (28)	$1\times1\times1$ (28)	37	57
	$1\times1\times2$ (56)	$1\times1\times2$ (56)	41	79
	$1\times1\times1$ (28)	$2\times2\times2$ (224)	56	81
	$1\times1\times2$ (56)	$2\times2\times2$ (224)	70	98
	$1\times1\times2$ (56)	$2\times2\times3$ (336)	69	97
	$1\times1\times2$ (56)	$3\times3\times4$ (1008)	69	99
β	$1\times1\times2$ (28)	$1\times1\times2$ (28)	40	166
	$1\times1\times2$ (28)	$2\times2\times4$ (224)	75	208
	$1\times1\times3$ (42)	$2\times2\times4$ (224)	71	194
	$1\times1\times3$ (42)	$2\times2\times5$ (280)	72	197
	$1\times1\times3$ (42)	$3\times3\times8$ (1008)	73	198
γ	$1\times1\times1$ (56)	$1\times1\times1$ (56)	75	
	$1\times1\times1$ (56)	$2\times2\times2$ (448)	81	
	$1\times1\times1$ (56)	$3\times3\times3$ (56)	82	

Uniform $\mathbf{k}$-point sampling meshes of $4\times4\times2$, $4\times4\times3$, and $3\times3\times3$ were used for the third-order IFCs of the α, β, and γ phases. For the former two phases the center of the a^*-b^* plane were sampled though the off-center grids along c^*-axis were sampled. For the γ phase, non-Γ center mesh was used. For the second-order IFC, the Γ-point was only sampled for the α and β phase supercells and the only one $\mathbf{k} = (0.5, 0.5, 0.5)$ point was sampled for the γ phase supercell. The $\mathbf{q}$-point sampling meshes of $14\times14\times16$, $14\times14\times32$, and $22\times22\times22$ were used to calculate the LTCs in Eq. (2) for the α, β, and γ phases.

To compare the calculated LTC with the experimental data measured at finite temperatures, the experimentally measured lattice parameters may be preferred in case that they are known. We examined LTC of β-Si$_3$N$_4$ at the equilibrium volumes ($V_\mathrm{eq}(T)$) within the quasi-harmonic approximation (QHA).[35] Except for this, the LTC values were calculated with the equilibrium volume at 0 K ($V_\mathrm{eq}(T = 0)$).

We calculated volumetric thermal expansion coefficients and compared them with the reported experimental values so as to check the validity of the present calculation, because the thermal expansion is originated from the anharmonicity of the interatomic potential as well as lattice thermal conduction. The calculated values are 4.31 and 4.19 (10^{-6} K^{-1}) at 300 K for the α and β phases, while the experimental values were 3.75 and 3.55 (10^{-6} K^{-1})[36]. The present calculation reproduced the experimental tendency where the α phase has a slightly larger thermal expansion coefficient than the β phase, supporting that the present calculations enable us to qualitatively compare the LTC values of the Si$_3$N$_4$ phases.

In order to compare the microscopic phonon properties among the three phases at the same conditions, those

results calculated at 0 GPa are shown and discussed. For the γ phase, this means that we assume the condition of virtually quenched γ phase at 0 GPa from the high pressure. To examine this, we calculated LTC of γ phase at 10, 20, and 40 GPa as shown in Fig. 8, where the phenomenological behaviour of linear dependence of LTC with respect to pressure with the calculated slope of 2.89 $Wm^{-1}K^{-1}GPa^{-1}$ was reproduced as similar to ref. 37. By this result, we consider that the microscopic values are also varied smoothly with the pressure and those at 0 GPa are meaningful to compare with the α and β phases.

C. Direct solution of LBTE

The merit of the single-mode RTA is that we can intuitively understand the qualitative character of LTC in terms of the relaxation time and group velocity. The microscopic understanding of the full solution of LBTE is still under the development (Andrea Cepellotti and Nicola Marzari Phys. Rev. X 6, 041013 (2016)) and the microscopic picture based on collective phonons (R.J. Hardy, Phys. Rev. B 2, 1193 (1970)) will require more complicate investigation although it is known that the single-mode RTA solution of LBTE underestimates the full solution.[20,24]

For the β phase, we partly adopted a direct solution of LBTE35, which is one of the methods of LBTE full solutions. Because of the larger computational demand for the direct solution, we calculated the LTC with the **q**-point sampling mesh of $10 \times 10 \times 26$. The LTC values of the direct solution without the isotope effect were 74 and 237 WK-1m-1 for κ_{xx} and κ_{zz}, respectively, while the corresponding single-mode RTA values were 74 and 205 $WK^{-1}m^{-1}$. The κ_{zz} of the direct solution was 16 % larger than that of the single-mode RTA solution. Since the LTC difference between the LBTE solutions is not significant and we expect the physics on LTC is well understood within RTA in the current level of our interest.

III. RESULTS AND DISCUSSION

A. Lattice thermal conductivities

In Table II, the theoretical LTCs at 300 K are compared with the previously reported experimental5,24,36 and theoretical16,17 values. The present calculation results better agree with the experimental κ_{xx} and κ_{zz} of β-Si$_3$N$_4$, compared with the references of the Slack model17 and MD16 results. The directional averages of the present κ_{ii} in the α, β, and γ phases are 79, 115, and 81 $Wm^{-1}K^{-1}$. The value of the γ phase is just as small as that of the α phase, although the former phase shows the largest bulk modulus (B) in Table II. It is generally known that simple models through Debye temperature can provide only their rough estimations. In section IV-C, we will investigate the detailed mechanisms of the

TABLE II. Calculated thermal conductivities of α-Si$_3$N$_4$ (trigonal), β-Si$_3$N$_4$ (trigonal), γ-Si$_3$N$_4$ (cubic), and wurtzite-type AlN (hexagonal) at 300 K, compared with the experimental data. Theoretical bulk moduli B in units of GPa, calculated by the authors by using the present band method, are presented in the fourth column.

	This work			Ref. Theo.			Ref. Expt.		
	κ_{xx}	κ_{zz}	B	κ	κ_{xx}	κ_{zz}	κ	κ_{xx}	κ_{zz}
α-Si$_3$N$_4$	69	99	224	70[a]	105[b]	225[b]	59[d]	-	-
β-Si$_3$N$_4$	73	198	237	250[a]	170[b]	450[b]	122[e]	69[f]	180[f]
γ-Si$_3$N$_4$	82	-	296	80[a]	-	-	-	-	-
w-AlN	218	190	196	-	240[c]	212[c]	285[g]	-	-

[a] Ref.17, Slack model
[b] Ref.16, molecular dynamics (Green-Kubo)
[c] Ref.23, LBTE full solution.
[d] Ref.24, thin film.
[e] Ref.5, poly-crystals.
[f] Ref.12, single crystalline grains of poly-crystals.
[g] Ref.36, single-crystal.

microscopic phonon properties behind the relative LTC values.

It can be seen that the theoretical LTCs of β-Si$_3$N$_4$ are markedly more anisotropic than those of the α phase. The theoretical LTCs of β-Si$_3$N$_4$ are in good agreement with the corresponding experimental data for individual grains reported by Li *et al.*12, indicates that the experimentally reported large anisotropy in the thermal conductivities of β-Si$_3$N$_4$ stems from the intrinsic properties of the crystal, rather than specific defects induced during the sample preparation process. Among the nitrides studied, the theoretical LTC of β-Si$_3$N$_4$ along the c axis (194 $WK^{-1}m^{-1}$) is the closest to the values for high-thermal-conductivity AlN.

Fig. 1 shows the theoretical LTCs of the α and β phases as a function of T, in comparison with the reference experimental data, which were measured from the polycrystalline samples. The data of the polycrystalline bulk samples cannot be directly compared with the theoretical LTC tensors because the microstructures of the bulk samples affect the thermal conductivities. We calculate theoretical LTC values of the polycrystalline bulk sample as $\kappa = w\kappa_{xx} + (1-w)\kappa_{zz}$, with an adjustable parameter w between 0 and 1 for the least square differences from the experimental data.

The temperature dependence of the theoretical LTC, induced by $\tau_{\lambda\text{ph-ph}}$, is close to T^{-1} because 300 K is high enough to approximate the linewidth in Eq. (1) by a high-temperature limit for these phases. In Fig. 1-a, the temperature dependence of the experimental data of a chemically vapor-deposited α-Si$_3$N$_4$ sample24 is deviated from T^{-1} considerably, intersecting the theoretical curves of the κ_{xx} and κ_{zz} at 400 and 600 K, respectively. Thus no value of w adjusts the theoretical LTC to the experimental curve. Assuming the underestimation of SMRTA $\sim$15 % from the results of the β phase, the full solution of
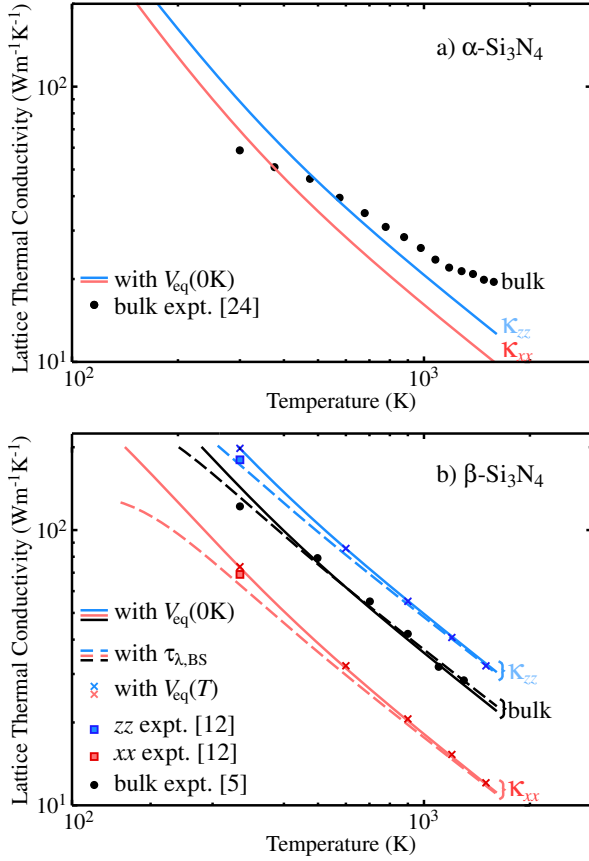
FIG. 1. (color online) Temperature dependence of LTC for α- and β-Si$_3$N$_4$. The LTC calculated with the fixed volume optimized at 0 K are shown by the solid curves. For β-Si$_3$N$_4$, the LTC with the boundary scattering effect are shown by broken curves. The LTC calculated with the equilibrium volumes at the temperatures are shown by crosses. Theoretical LTC for the bulk β-Si$_3$N$_4$ sample are also shown to be compared with the experimental LTC (filled circles) of the bulk sample.

LBTE would cure the disagreement only partly. Including the simple phonon lifetime of boundary scattering, $\tau_{\lambda,\text{BS}} = L/v_\lambda$, into the total phonon lifetime according to Matthiessen's rule, could not explain the discrepancy as well. $\tau_{\lambda,\text{BS}} = L/v_\lambda$ with $L = 0.75$ μm, which was much smaller than the experimental grain size 10 μm, decreases the room-temperature theoretical κ_{xx} and κ_{zz} values toward the experimental value, but severely underestimated the experimental values at the high temperature side. At present, the reason for the discrepancy between the theoretical and experimental behaviors is unclear. Although the crystal structure of the experimental sample was characterized as α-Si$_3$N$_4$, significant lattice defects might exist in the as-deposited sample as pointed out by Hirosaki *et al.*16, and many of them might be diminished in the high temperature side of the measurement.

The experimental values of the β-phase ceramic bulk5 fall well between the calculated values of κ_{xx} and κ_{zz}.

The experimental data are nearly parallel to the theoretical κ_{xx} and κ_{zz} curves. If we compare the experimental values with $\sum_i \kappa_{ii}/3$, which is a simple directional average, the calculation shows slight underestimations with respect to the experiment, which can be understood from an experimentally tailored microstructure containing large β-Si$_3$N$_4$ grains selectively grown along the c axis5.

The theoretical curve adjusted with $w = 0.37$ explains well the experimental data of the poly-crystal bulk in Fig. 1-b. For the effects of lattice defects most of which are grain boundaries, we included $\tau_{\lambda,\text{BS}}$ with $L = 1$ μm to further fit the theoretical curve ($w = 0.44$) to the experimental data. The L value is similar to the average grain size (2 μm) of the experimental polycrystalline sample5. Fig. 1-b also contains the experimental κ_{xx} and κ_{zz} at room temperature by filled squares, which are in-between the theoretical components with and without $\tau_{\lambda,\text{BS}}$.

The LTC values with the equilibrium lattice volumes (V_{eq}) at 300, 600, 900, 1200 and 1500 K within QHA are plotted by crosses in Fig. 1. The deviations due to the thermal expansions were less than 1 %. Therefore this effect is negligible for the present study. The degree of the differences is similar to the case of Si and Ge21.

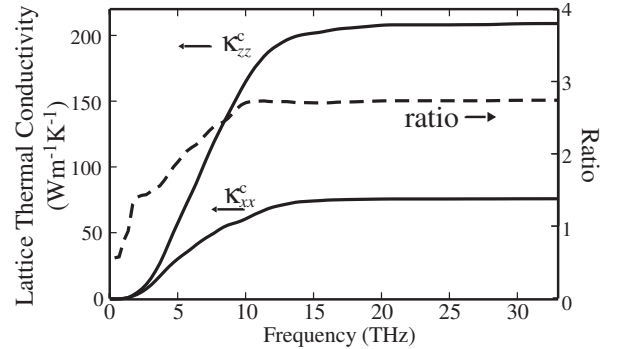## B. Distributions of phonon frequencies of α and β phases in Brillouin zones

FIG. 2. Theoretical cumulative sums of mode LTC $\kappa^{\text{c}}(\omega)$ (see Eq. (3)) of β-Si$_3$N$_4$ along the a and c axes, i.e., $\kappa_{xx}^{\text{c}}(\omega)$ and $\kappa_{zz}^{\text{c}}(\omega)$, respectively, and their ratios, $\kappa_{zz}^{\text{c}}(\omega)/\kappa_{zz}^{\text{c}}(\omega)$.

Fig. 2 shows the $\kappa^{\text{c}}(\omega)$ of the β phase along two inequivalent directions and their ratios as an indicator of the anisotropic thermal conductivities; isotope effects are not considered in this figure. We can clearly see that the phonon modes in the frequency range of 012 THz contribute significantly to LTC. Interestingly, in the same frequency range, the anisotropy of $\kappa^{\text{c}}(\omega)$ increases monotonically. Thus, we can focus on this frequency range when we investigate the anisotropy of the thermal conductivity of the β phase in detail.

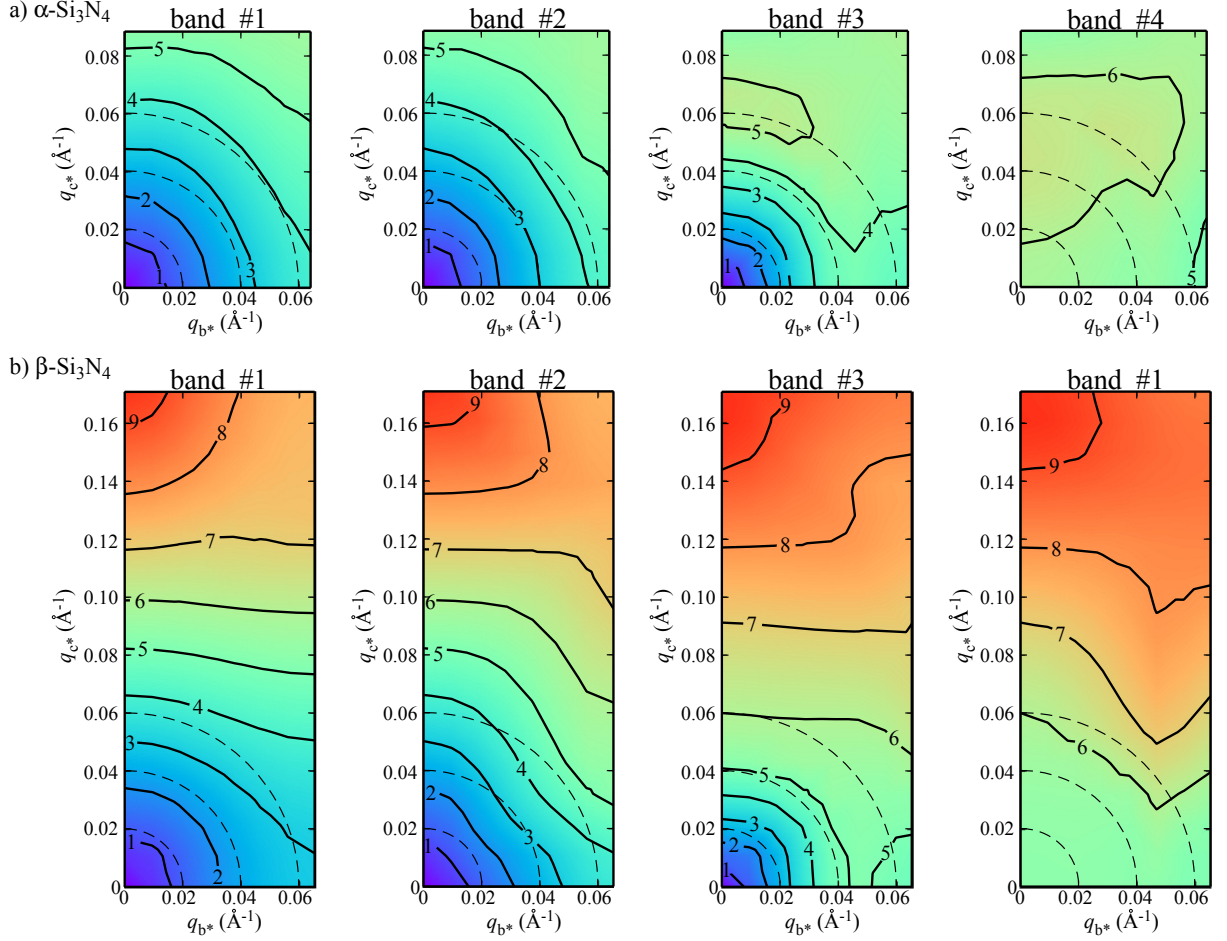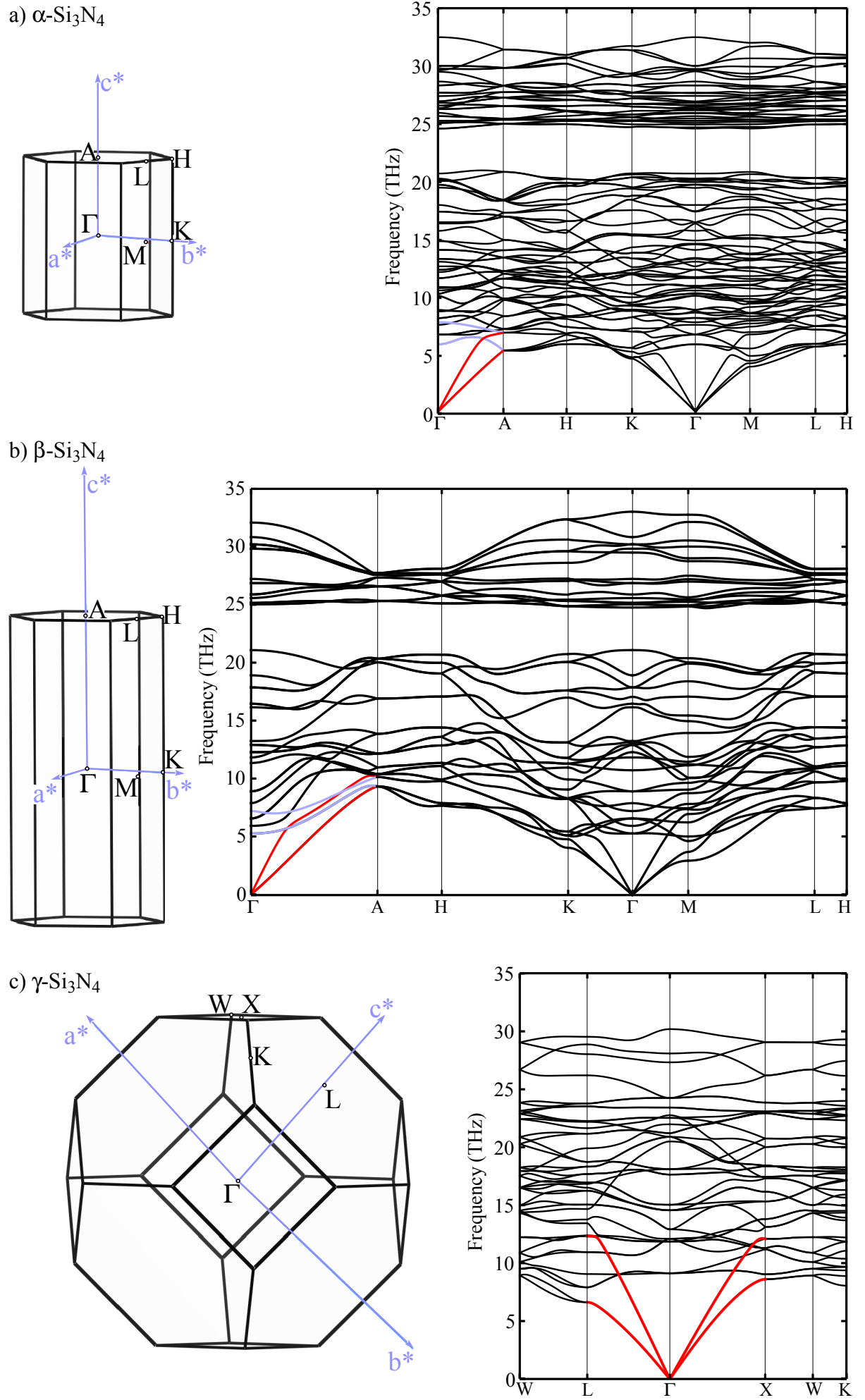The cross-sections of the phonon frequency distribu-

FIG. 3. (color online) Contour maps of phonon frequency (THz) on the b^*-c^* planes of Brillouin zones. The maps for the four lowest-frequency phonon states are shown. The frequency landscapes are formed by simply connecting the frequencies of the same band indices, assigned by ascending order of frequency at the respective q points.

tions on the b^*-c^* planes in the first Brillouin zones are shown in Fig. 3. The cross-sections of other planes containing the c^* axis did not differ much from Fig. 3; thus, we focus on the results for the b^*-c^* planes as representative of all such planes. We show only the frequencies of four modes from the lowest frequency because they contribute significantly to LTC. In Fig. 3-b of the β phase, the iso-frequency lines in $0.06 \leq q_{c^*} \leq 0.12$ (Å^{-1}) are almost parallel to the q_{b^*} axis, i.e., the group velocities in this section are nearly along the c axis. The cross-sections in Fig. 3-b indicate that the four modes of the β phase, in a significantly large part of the phonon states in the Brillouin zone, have group velocities oriented along the c axis, resulting in a much larger LTC along the c axis than along the a (b) axis in this phase. Fig. 3-a shows that the frequency distributions and group velocities of α-Si$_3$N$_4$ are fairly isotropic.

C. Harmonic phonon states

Figure 4 shows the phonon band diagrams of the three Si$_3$N$_4$ phases. Among the four terms in Eq. (3), we qualitatively investigate the contributions of v_λ and DOS to LTC. The entire band diagrams and DOSs are almost identical to those reported earlier[37,38]. However, the focused points in the previous works were different from the present study. The previous works investigated the entire DOS spectra to understand the relative thermodynamic stability among the phases and thus did not refer to our noted differences in the phonon states responsible for LTC, i.e., those in 0-12 THz.

In the band diagram of β (Fig. 4-b), along the Γ-A path, the acoustic phonon branches highlighted in red increase their frequencies almost linearly from the Γ-point to the zone boundary of the A-point around 10 THz. Their gradients are large, so the group velocity components along the c axis maintain high values. Normally, optical branches are flat; however, the upper branches

a) α-Si₃N₄

b) β-Si₃N₄

c) γ-Si₃N₄

FIG. 4. (color online) Brillouin Zones (left), calculated phonon band diagrams (right) for the three Si₃N₄ phases.

along the same path, highlighted in blue, also have significantly large group velocity components along the c axis.

In contrast, the corresponding acoustic branches in the α phase highlighted in red in Fig. 4-a do not increase their frequencies as much as those of the β phase. This is because the Γ-A path length of the α phase is approximately half that of β. The lattice constant c of α is nearly twice that of β, owing to the difference in the stacking manner of the basal layers. The frequency maxima along the Γ-A path are around 7 THz, rather close to the maxima along the Γ-K and Γ-M paths (around 5 THz). Moreover, the upper branches highlighted in blue are relatively flat, like the upper branches along the Γ-K and Γ-M paths.

The total DOS of the α phase shows a distinct peak at 6 THz, as indicated by an arrow, where the phonon branches become dispersionless over the entire path in the band diagram. The first peaks of α and β are related to the L-points or the Brillouin zone (BZ) edges with $c^* = 0.5$. The difference in their frequencies stems from difference in length between their BZs along c^*.

In the DOS projected onto the c and a axes (PDOS) shown in the insets of the total DOS, the two PDOS spectra of the β phase have a larger difference than in the case of α, which is consistent with the differences in the dispersion curves. Note that the previous studies did not refer to the difference of PDOS between the two phases.

In the band diagram of the γ phase (Fig. 4-c), the acoustic phonon branches highlighted in red show significant linear dispersion along the L-Γ-X path. The frequencies of the longitudinal acoustic modes are 14 and 12.5 THz at the L- and X-points. The frequencies of the transverse acoustic modes are approximately half the values of the longitudinal modes at the L-point and a factor of $1/\sqrt{2}$ smaller than the longitudinal modes at the X-point, as in the case of fcc rare gas solids39. The roughly constant gradients of the branches are large, reflecting the large elastic constants of the γ phase as shown in Table II. The DOS in the frequency range of 0-5 THz, where only acoustic modes exist, is thus rather small. By fitting the total DOS with a Debye model function, $a_D\omega^2$, the coefficient a_D of the γ phase is rather small. They are 10×10^{-3}, 9.1×10^{-3}, and 3.9×10^{-3} (THz^{-3}formula^{-1}) for the α, β, and γ phases, respectively. The maximum frequencies of the Debye model for the three phases, $\nu_D = \left(\frac{9}{Za_D}\right)^{1/3}$, are 6.0, 7.9 and 10.5 THz, respectively, where Z is the number of molecules in the primitive cell. In the next section, the largest ν_D in the γ phase will be related to the phonon lifetimes to explain why the γ phase has a relatively small LTC.
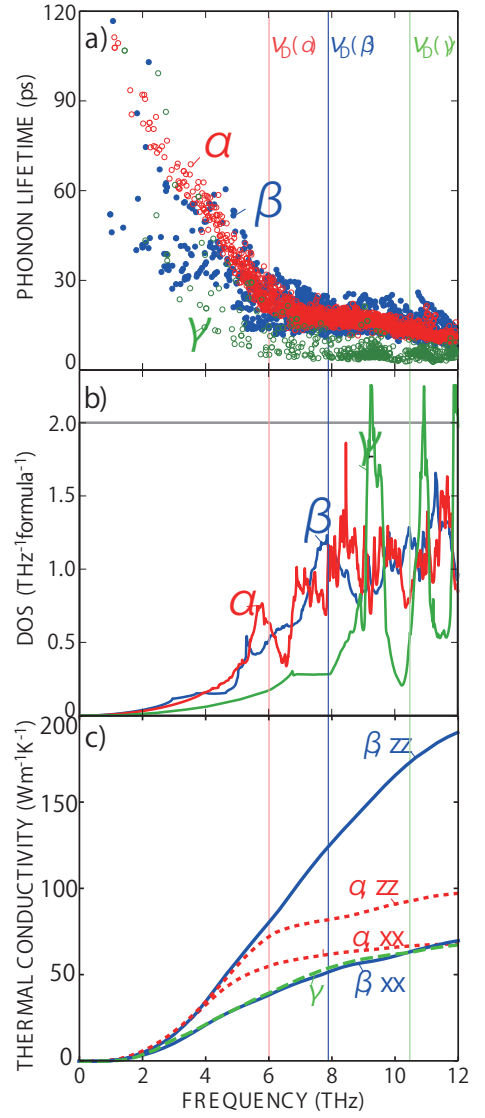

FIG. 5. (color online) Frequency-distributions of phonon lifetimes (a), DOS, (b) and cumulative thermal conductivities (c) among the three Si$_3$N$_4$ phases.

D. Distributions of phonon lifetimes and their impact on the LTCs of the three phases

The distributions of the phonon lifetimes are shown in Fig. 5-a. The DOS and cumulative thermal conductivities are attached in Fig. 5-b and c, to allow the distributions of the phonon states and their contributions to LTC to be examined with ease. The common trend is that the phonon lifetime decreases with increasing ω in the lower frequency region (< 6 THz). Most of the phonon lifetimes of the α phase are larger than those of the β phase in this frequency region. However, above 6 THz, the phonon lifetimes of the three phases are distributed similarly and roughly constant. The values for γ are as low as half those for α and β. The vertical lines in Fig. 5

show the maximum frequencies of the Debye model, ν_D. We use ν_D as a roughly estimated frequency-boundary between the acoustic and optical phonon modes. From Fig. 5 and the band diagrams of Fig. 4, we can highlight the frequency-dependent microscopic mechanisms on 1) the large κ_{zz} of the β phase, and 2) the relatively small LTC value of the γ phase.

Only the zz component of $\boldsymbol{\kappa}^c(\omega)$ for the β phase increases much as increases beyond ν_D. It is a characteristic point of the β phase that the phonon modes of $\omega > \nu_D$ largely contribute to the κ_{zz}. They contribute approximately $1/3$ of the total κ_{zz}. Because the phonon lifetimes in this frequency range are not large, a large number of phonon modes with large z components of group velocities, including optical phonon modes like the upper branches highlighted by blue in Fig. 4, contribute to the κ_{zz}. In contrast to the β phase, the zz component of the α phase does not increase much above ν_D, as all the phonon branches reach to the Brillouin zone boundary and decreased their group velocities.

The γ phase has the largest ν_D, and the smallest phonon lifetimes above 6 THz. Thus the frequency-distributions of the acoustic phonon states and their life-times of the γ phase are least compatible for high LTC among the three phases, while the optical phonon modes do not have large group velocities. This is the reason for the relatively small LTC of the γ phase in spite of the large group velocities of the acoustic branches.
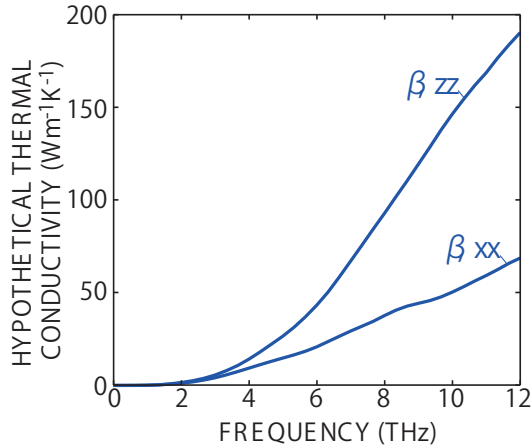
FIG. 6. (color online) Hypothetical cumulative thermal conductivity for β-Si$_3$N$_4$.

Our argument that the anisotropic group velocities are responsible for the anisotropic LTC of the β phase can be simply confirmed by hypothetically setting the two (C_λ and τ_λ) of the microscopic four terms (C_λ, v_λ, τ_λ, and DOS) constant. In Fig. 6 are the corresponding hypothetical cumulative thermal conductivities,

$$\boldsymbol{\kappa}^{c'}(\omega) = \frac{k_B \tau}{N_q \Omega} \int_0^\omega \sum_\lambda \mathbf{v}_\lambda \otimes \mathbf{v}_\lambda \delta(\omega' - \omega_\lambda) d\omega' \quad (4)$$

The mode heat capacity was set to Boltzmanns constant, k_B, as the high-temperature approximation, which is a reasonable approximation for $\omega < 19$ THz, and we set τ to 20 ps and let the of the β phase approach at $\omega = 12$ THz for simplicity. $\boldsymbol{\kappa}^{c'}(\omega)$ shows as large anisotropy as $\boldsymbol{\kappa}^c(\omega)$, confirming that the anisotropy in LTC is caused by the anisotropic group velocities while insensitive to the distribution of phonon lifetimes.
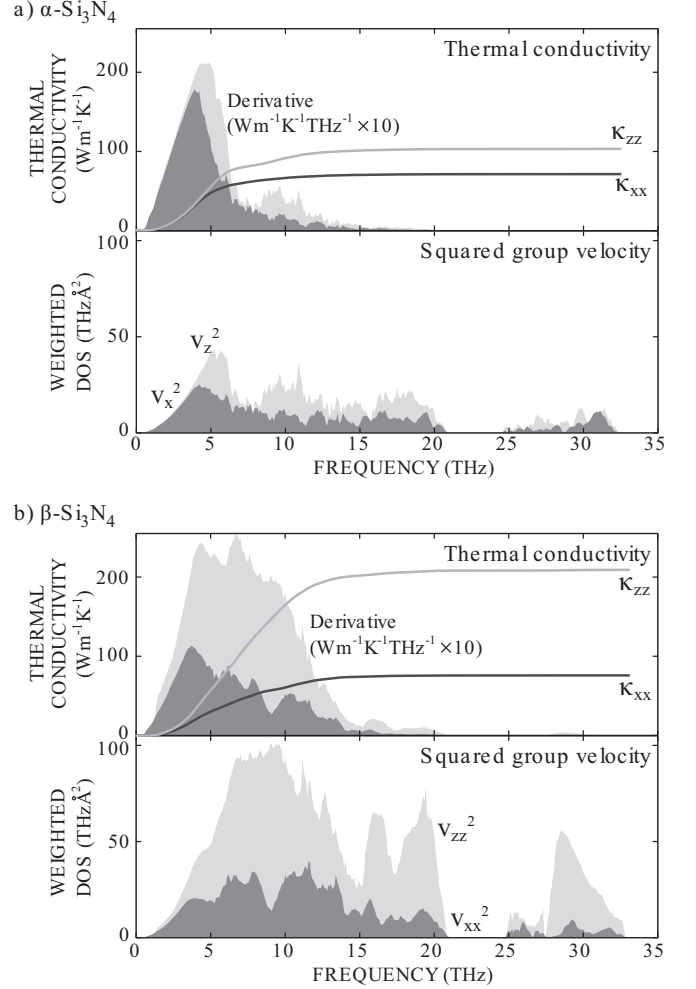
FIG. 7. (color online) Comparison between derivatives of cumulative thermal conductivity and DOS weighted with squared group velocity. a) α-Si$_3$N$_4$ and b) β-Si$_3$N$_4$.

Moreover, to clearly show the different degrees of the anisotropy between α- and β-Si$_3$N$_4$, in Fig. 7, we compare the derivative of the cumulative thermal conductivity, $d\boldsymbol{\kappa}^c/d\omega$, with the DOS weighted with the squared group velocity. The intensities of the latter is calculated by

$$v_{ii}^2(\omega) = \frac{1}{N_q \Omega} \sum_\lambda \mathbf{v}_{\lambda,i}^2 \delta(\omega - \omega_\lambda) \quad (5)$$

For both of α- and β- Si$_3$N$_4$, we can see the similarity between the derivatives of κ_{zz} and κ_{xx} with the DOS

weighted with $v_{\lambda,z}^2$ and $v_{\lambda,x}^2$. For the higher frequencies than approximately 15 THz, the mode heat capacities decrease and suppress the intensities of the derivatives. The areal intensity of the derivatives and the weighted DOS are consistent for the lower frequency region. Therefore the difference in the anisotropy of the LTC between the α and β phases reflects the difference in the group velocities, which is originated from the difference in the stacking order of the basal planes.

ACKNOWLEDGMENTS

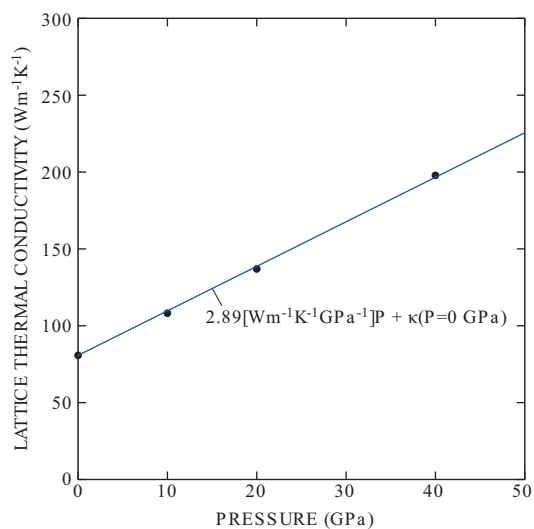**Appendix A: Pressure dependence of LTC of γ-phase**

FIG. 8. (color online) Pressure dependence of LTC of γ-Si$_3$N$_4$.

* k-tatsumi@imass.nagoya-u.ac.jp
[1] G. Slack, Journal of Physics and Chemistry of Solids **34**, 321 (1973).
[2] Y. Zhou, H. Hyuga, D. Kusano, Y.-i. Yoshizawa, and K. Hirao, Advanced Materials **23**, 4563 (2011).
[3] K. Hirao, K. Watari, H. Hayashi, and M. Kitayama, MRS Bulletin **26**, 451 (2001).
[4] K. Watari, Journal of the Ceramic Society of Japan **109**, S7 (2001).
[5] N. Hirosaki, Y. Okamoto, M. Ando, F. Munakata, and Y. Akimune, Journal of the Ceramic Society of Japan **104**, 49 (1996).
[6] F. L. Riley, Journal of the American Ceramic Society **83**, 245 (2000).
[7] S. Hampshire, H. Park, D. Thompson, and K. Jack, Nature **274**, 880 (1978).
[8] M. Yashima, Y. Ando, and Y. Tabira, The Journal of Physical Chemistry B **111**, 3609 (2007).
[9] D. Du Boulay, N. Ishizawa, T. Atake, V. Streltsov, K. Furuya, and F. Munakata, Acta Crystallographica Section B: Structural Science **60**, 388 (2004).

[10] A. Zerr, G. Miehe, G. Serghiou, M. Schwarz, E. Kroke, R. Riedel, H. Fueß, P. Kroll, and R. Boehler, Nature **400**, 340 (1999).

[11] Y. Zhang, A. Navrotsky, and T. Sekine, Journal of materials research **21**, 41 (2006).

[12] B. Li, L. Pottier, J. Roger, D. Fournier, K. Watari, and K. Hirao, Journal of the european ceramic society **19**, 1631 (1999).

[13] T. Takahashi, M. Sado, N. Sugimoto, J. Tatami, M. Iijima, S. Inagaki, Y. Kubota, I. Yamamoto, and S. Tanaka, Advanced Powder Technology **27**, 2005 (2016).

[14] Y. Yamamoto, N. Hirosaki, I. Ishikawa, J. YE, K. Matsuo, K. Furuya, F. Munakata, and Y. Akimune, Journal of the Ceramic Society of Japan **108**, 515 (2000).

[15] K. Watari, L. Pottier, B. Li, D. Fournier, and M. Toriyama, Ceramic Transactions(USA) **118**, 341 (2000).

[16] N. Hirosaki, S. Ogata, C. Kocer, H. Kitagawa, and Y. Nakamura, Physical Review B **65**, 134110 (2002).

[17] D. Morelli and J. Heremans, Applied physics letters **81**, 5126 (2002).

[18] D. Broido, M. Malorny, G. Birner, N. Mingo, and D. Stewart, Applied Physics Letters **91**, 231922 (2007).

[19] I. O. Thomas and G. Srivastava, Physical Review B **86**, 045205 (2012).

[20] A. Ward and D. Broido, Physical Review B **81**, 085205 (2010).

[21] K. Esfarjani, G. Chen, and H. T. Stokes, Physical Review B **84**, 085204 (2011).

[22] A. Togo, L. Chaput, and I. Tanaka, Physical Review B **91**, 094306 (2015).

[23] T. Hirai, S. Hayashi, and K. Niihara, AM. CERAM. SOC. BULL. Am. Ceram. Soc. Bull. **57**, 1126 (1978).

[24] S. Mukhopadhyay, L. Lindsay, and D. J. Singh, Scientific reports **6** (2016).

[25] S.-i. Tamura, Physical Review B **27**, 858 (1983).

[26] A. Togo and I. Tanaka, Scripta Materialia **108**, 1 (2015).

[27] P. E. Blöchl, Phys. Rev. B **50**, 17953 (1994).

[28] G. Kresse and J. Furthmüller, Physical review B **54**, 11169 (1996).

[29] G. Kresse, J. Non-Cryst. Solids **193**, 222 (1995).

[30] D. J. Kresse, Georg, Phys. Rev. B **59**, 1758 (1999).

[31] J. P. Perdew, K. Burke, and M. Ernzerhof, Physical review letters **77**, 3865 (1996).

[32] W. Paszkowicz, R. Minikayev, P. Piszora, M. Knapp, C. Bähtz, J. Recio, M. Marques, P. Mori-Sánchez, L. Gerward, and J. Jiang, Physical Review B **69**, 052103 (2004).

[33] D. M. Ceperley and B. Alder, Physical Review Letters **45**, 566 (1980).

[34] S. Wei and M. Chou, Physical review letters **69**, 2799 (1992).

[35] M. T. Dove, Introduction to lattice dynamics, Vol. 4 (Cambridge university press, 1993) pp. 76–77.

[36] P. P. M. K. R. Minikayev, W. Paszkowicz and C. Bähtz, "Thermal expansion of and silicon nitride," (2007).

[37] P. Andersson, Journal of Physics C: Solid State Physics **18**, 3943 (1985).